This document is the Accepted Manuscript version of a Published Work that appeared in final form in Organic Electronics 26 (2015) 36–47 http://dx.doi.org/10.1016/j.orgel.2015.07.014

Efficient solution processed D_1-A-D_2-A-D_1 small molecules bulk heterojunction solar cells based on alkoxy triphenylamine and benzo[1,2-b:4,5-b^0]thiophene units

Challuri Vijay Kumar [a], Lydia Cabau [a], Emmanuel N. Koukaras [b], Ganesh D. Sharma [c,⇑], Emilio Palomares [a,d,⇑]

[a] Institute of Chemical Research of Catalonia (ICIQ), Avda. Països Catalans 16, E-43007 Tarragona, Spain
[b] Molecular Engineering Laboratory, Department of Physics, University of Patras, Patras 26500 GR, Greece
[c] R & D Center for Engineering and Science, JEC Group of Colleges, Jaipur Engineering College, Kukas, Jaipur 303101, India
[d] Catalan Institution for Research and Advance Studies (ICREA), Avda. Lluis Companys 23, E-08010 Barcelona, Spain

a b s t r a c t

Two molecules denoted as VC96 and VC97 have been synthesized for efficient (g = 6.13% @ 100 mW/cm^2 sun-simulated light) small molecule solution processed organic solar cells. These molecules have been designed with the D_1-A-D_2-A-D_1 structure bearing different central donor unit, same benzothiadiazole (BT) as p-acceptor and end capping triphenylamine. Moreover, the optical and electrochemical properties (both experimental and theoretical) of these molecules have been systematically investigated. The solar cells prepared from VC96:$PC_{71}BM$ and VC97:$PC_{71}BM$ (1:2) processed from CF (chloroform) exhibit a PCE (power conversion efficiency) of g = 4.06% (J_{sc} = 8.36 mA/cm^2, V_{oc} = 0.90 V and FF = 0.54) and g = 3.12% (J_{sc} = 6.78 mA/cm^2, V_{oc} = 0.92 V and FF = 0.50), respectively. The higher PCE of the device with VC96 as compared to VC97 is demonstrated to be due to the higher hole mobility and broader IPCE spectra. The devices based on VC96:$PC_{71}BM$ and VC97:$PC_{71}BM$ processed with solvent additive (3 v% DIO, 1,8-diiodooctane) showed PCE of g = 5.44% and g = 4.72%, respectively. The PCE device of optimized VC96:$PC_{71}BM$ processed with DIO/CF (thermal annealed) has been improved up to 6.13% (J_{sc} = 10.72 mA/cm^2, V_{oc} = 0.88 V and FF = 0.61). The device optimization results from the improvement of the balanced charge transport and better nanoscale morphology induced by the solvent additive plus the thermal annealing.

1. Introduction

Over the last decade, solution processed organic solar cells (OSCs) have received the interest of the scientific community, owing to their facile fabrication via printing technologies such as roll to roll, inkjet and doctor blade methods that hold the promise for low cost and efficient mass production [1–3]. The device architecture that most commonly used in the OSCs is the bulk heterojunction (BHJ), consists of a blend of a photoactive layer narrow bandgap (usually conjugated polymer or small molecule) donor material and soluble fullerene acceptor [4,5]. With the rapid progress over recent years, power conversion efficiencies (PCEs) over 9% have been achieved for polymer based OSCs [6–9]. Although OSCs based on low bandgap conjugated polymers have revealed outstanding performances, are still expensive, suffering from complex steps for purification with respect to polydispersity and have large batch to batch variation as compared to small molecules. In this regard, p-conjugated organic semiconductors are attractive single-junction solution processed BHJ small molecule solar cells [10–16] due to various advantages over their polymer counterparts, such as well defined molecular structures, definite molecular weight, easy synthetic processes and also easier purification techniques. The PCEs in the range of 6–10% have been achieved in recent years for a single BHJ solar cell [17–22] and a PCE of 10.1% [23] and 12% for tandem cell devices [24].

To achieve high PCE with a small molecule OSCs, low bandgap small molecules containing alternating D (electron donor) and A

⇑ Corresponding authors at: Institute of Chemical Research of Catalonia (ICIQ), Avda. Països Catalans 16, E-43007 Tarragona, Spain (E. Palomares).
E-mail addresses: gdsharma273@gmail.com, sharmagd_in@yahoo.com (G.D. Sharma), epalomares@iciq.es (E. Palomares).

(electron acceptor) units in the backbone or side chains have been extensively designed and synthesized because of the easily tunable energy levels and solubility [25,26]. Among them, benzo[1,2-b:4,5-b′]dithiophene (BDT) unit is a good electron donating group and has been the figure of merit recently as an attractive donor building block in organic semiconductor materials for high performance OSCs because of its rigid coplanar fused ring structure, which easily gives rise to high p-electron delocalization and strong intermolecular p–p stacking [27,28]. Moreover, introduction of a thiophene unit onto the BDT side position (BDTT) as means to extend for the molecular p-overlap, improves the charge transport, without affecting charge recombination, leading to a high J_{sc} [29–32]. Moreover, as a relatively weak donor, BDT would maintain a deeper highest occupied molecular orbital (HOMO) energy level of the resulting small molecules [33,34]. By tailoring the core, peripheral groups, and conjugated bridges with various donors and acceptor units, SM based solar cells with high PCE could be achieved.

In this work, we report the synthesis and characterization (optical and electrochemical) of two symmetrical D_1-A-D_2-A-D_1 organic small molecules denoted as VC96 and VC97 consisting of 4,8-bis[5-(2-ethylhexyl)thiophen-2-yl]benzo[1,2-b:4,5-b′]-dithiophene and dialkoxy-substituted 4,8-bis[(2-ethylhexyl)oxy]benzo[1,2-b:4,5-b′]dithiophene central core donor units, respectively and same benzothiadiazole unit as acceptor and dihexyloxy-substituted triphenylamine (DHO-TPA) donor unit as end capping units. The BDT and BDTT were selected as donor core because of their relatively large and planar conjugated structure and could enhance the p-conjugation degree and increase hole mobility. Moreover, TPA electron donating unit plays an important role in stabilizing the separated hole from the exciton and improves the transporting properties of charge carrier [35–40]. The alkoxy substituted triarylamine end cap units are also incorporated to extend the p-conjugated structure to improve solubility and film forming properties. These two small molecules were used as donor along with $PC_{71}BM$ as electron acceptor for the fabrication of solution processed BHJ small molecule solar cells. The devices based on VC96:$PC_{71}BM$ and VC97:$PC_{71}BM$ (1:2) spin cast from chloroform solvent, resulted PCE of 4.06% and 3.12%, respectively. In an attempt to improve the PCE, we have adopted solvent additive (SA), i.e., 3% v DIO/CF technique and achieved PCE of 5.44% and 4.72%, for VC96:$PC_{71}BM$ and VC97:$PC_{71}BM$ active layer, respectively. The PCE has been further optimized to 6.13%, when DIO/CF processed VC96:$PC_{71}BM$ was thermally annealed at 110 oC for 10 min. The enhancement in the PCE with SA and thermally annealed SA based device is attributed to the balanced charge transport, higher light harvesting ability, and better nanoscale morphology for exciton dissociation and charge transport and collection.

2. Experimental details

2.1. Materials

Unless stated otherwise, all reagents were purchased from commercial sources and used without further purification. $Pd(PPh_3)_4$, $B(OCH_3)_3$ and n-butyllithium (2.0 M in hexane) were purchased from Sigma–Aldrich©. Dry THF (tetrahydrofuran) and toluene were obtained by passing them through an activated alumina column on a PureSolv™ solvent purification system (Innovative Technologies, Inc., MA). N,N-Bis(4-hexyloxyphenyl)-4-bromoaniline (1) [41] 6-bis(tributylstannyl)-4,8-bis(5-(2-ethylhexyl)thiophen-2-yl)benzo[1,2-b:4,5-b′]dithiophene [18], 2,6-bis(trimethylstannyl)-4,8-bis(2-ethylhexoxy)benzo-[1,2-b:4,5-b′]dithiophene [42] was synthesized as per the earlier reported procedure.

2.2. Methods

The UV–Vis absorption spectra were measured in a 1 cm quartz cell using a Shimadzu© model 1700 spectrophotometer. The steady state fluorescence spectra were recorded using a Spex model Fluoromax-3 spectrofluorometer using a 1 cm quartz cell. All ^1H and ^{13}C NMR spectra were recorded on a Bruker AV 300 and AV 500 instruments, respectively, at a constant temperature of 300 K, unless otherwise stated. ^1H spectra were referenced to tetramethylsilane. The ESI (Electro Spray Ionization) mass spectra were recorded on a Water Quattro micro (Water Inc, USA). The cyclic voltammetric experiments were carried out with a PC-controlled CH instruments model CHI620C electrochemical analyzer. The flash column chromatography was carried out using Silica gel 60, 40–63 1m (Panreac Química SLU) as the stationary phase. The size exclusion chromatography was carried out in a large elution column (1000 mm x 38 mm) with Biobead SX3 (Bio-Rad Laboratories, Inc.) as the stationary phase. The eluent was passed through the column under gravity.

2.3. Synthesis of VC96 and VC97

2.3.1. Synthesis of N-(4-(4-bromobenzo[c][1,2,5]thiadiazol-7-yl)-phenyl)-4-(hexyloxy)-N(4(hexyloxy)phenyl)benzenamine (3)

N,N-Bis(4-hexyloxyphenyl)-4-bromoaniline (compound 1) (0.385 g, 0.734 mmol) was added to a round flask with 20 mL of THF and was stirred under nitrogen atmosphere at −78 oC. nBuLi 2 M in hexane (0.08 mL, 0.859 mmol) was added and the mixture was stirred for 15 min at −78 oC. After that, $B(OMe)_3$ (0.12 mL, 1.10 mmol) was added and the reaction was stirred overnight at −78 oC. The crude was warmed at room temperature. In another Schlenk, $Pd(PPh_3)_4$ (0.023 g, 0.02 mmol), 4,7-dibromobenzothiadiazole (2) (0.193 g, 0.66 mmol), K_2CO_3 2 M (3 mL). The borate crude material and THF (20 mL) was added and the reaction was stirred at 70 oC for 6 h. Then water was added. The crude product was extracted into $CHCl_3$, and the organic layer was dried over Na_2SO_4. The residue was purified by silica gel column chromatography (hexane/dichloromethane 6:4) to obtain a purple solid (0.450 g, 63% yield). ^1H NMR (300 MHz, $CDCl_3$) d_H 7.83 (d, J = 7.9 Hz, 1H), 7.71 (d, J = 7.9 Hz, 2H), 7.47 (d, J = 7.9 Hz, 1H), 7.08 (d, J = 8.8 Hz, 4H), 6.99 (d, J = 8.8 Hz, 2H), 6.81 (d, J = 9.7 Hz, 4H), 3.92 (t, 4H), 1.74 (m, 2H), 1.28 (m, 12H), 0.85 (m, 6H). MS-ESI (m/z): $[M]^+$ calculated for 680.1915.

2.3.2. Synthesis of 2,6-bis(N-(4-(4-bromobenzo[c][1,2,5]thiadiazol-7-yl)phenyl)-4-(hexyloxy)-N(4(hexyloxy)phenyl)benzenamine-4,8-bis(5-(2-ethylhexyl)thiophen-2-yl)benzo[1,2-b:4,5-b′]dithiophene (VC96)

A solution of 3 (152 mg, 0.242 mmol) and 2,6-bis(tributylstannyl)-4,8-bis(5-(2-ethylhexyl)thiophen-2-yl)benzo[1,2-b:4,5-b′]dithiophene (4) (100 mg, 0.110 mmol) in dry toluene (20 mL) was degassed twice with argon followed by the addition of $Pd(PPh_3)_4$ (12 mg, 0.1 mmol). After being stirred at 120 oC for 48 h, the reaction mixture was poured into water and extracted with CH_2Cl_2. The organic layer was washed with water and then dried over $MgSO_4$. After removal of solvent, the crude product was purified by column chromatography on silica gel using CH_2Cl_2 and hexane (1:1) as eluent and subsequent size exclusion chromatography using THF as eluent to obtain a purple solid (115 mg, 63%). ^1H NMR (500 MHz, $CDCl_3$) d_H: 8.80 (s, 2H), 7.94 (d, J = 7.1 Hz, 2H), 7.81 (d, J = 9.9 Hz, 4H), 7.65 (d, J = 8.5 Hz, 2H), 7.50 (d, J = 4.3 Hz, 2H), 7.12 (d, J = 9.9 Hz, 8H), 7.04 (m, 6H), 6.87 (d, J = 7.1 Hz, 8H), 3.97 (m, 8H), 2.96 (t, 4H), 1.81 (m, 10H), 1.49–1.37 (m, 40H), 1.04–0.94 (m, 24H). ^{13}C NMR (100 MHz, $CDCl_3$) d: 155.84, 154.06, 149.24, 145.86, 140.36, 130.83, 137.98, 129.74, 128.47, 127.66, 127.10, 123.54, 125.57, 125.28, 124.56, 124.06, 119.52, 115.34, 68.29,

41.58, 34.35, 32.60, 31.63, 25.78, 23.11, 22.63, 22.63, 14.23, 14.05, 11.07. MALDI: m/z calcd for [M]+, 1732.7924 (^{1}H NMR/^{13}C NMR and MALDI-TOF spectra are shown in Supporting information). Anal. Calcd. for $C_{106}H_{120}N_6O_4S_6$ C, 73.40; H, 6.97; N, 4.85; S, 11.09. Found C, 71.55; H, 6.80; N, 4.51; O, 10.69.

2.3.3. Synthesis of 2,6-bis(N-(4-(4-bromobenzo[c][1,2,5]thiadiazol-7-yl)phenyl)-4-(hexyloxy)-N-(4(hexyloxy)phenyl)benzenamine)-4,8-bis(2-ethylhexyloxy)benzo-[1,2-b:4,5-b′]dithiophene (VC97)

A solution of 3 (186 mg, 0.284 mmol) and 2,6-bis(trimethylstannyl)-4,8-bis(2-ethylhexoxy)benzo-[1,2-b:4,5-b′]dithiophene (5) (100 mg, 0.129 mmol) in dry toluene (20 mL) was degassed twice with argon followed by the addition of $Pd(PPh_3)_4$ (15 mg, 0.1 mmol). After being stirred at 120 oC for 48 h, the reaction mixture was poured into water and extracted with CH_2Cl_2. The organic layer was washed with water and then dried over $MgSO_4$. After removal of solvent, the crude product was purified by column chromatography on silica gel using CH_2Cl_2 and hexane (1:1) as eluent and subsequent size exclusion chromatography using THF as eluent to obtain a purple solid (120 mg, 65%). ^{1}H NMR (500 MHz, $CDCl_3$) d_H: 8.8 (s, 2H), 7.97 (d, J = 6.2 Hz, 2H), 7.83 (d, J = 10.4 Hz, 4H), 7.77 (d, J = 10.4 Hz, 2H), 7.11 (m, 8H), 7.04 (d, J = 9.2 Hz, 4H), 6.84 (m, 8H), 4.33 (m, 4H), 3.93 (t, 8H), 1.90 (m, 2H), 1.77 (m, 14H), 1.45 (m, 16H), 1.34 (m, 18H), 1.10 (m, 6H), 0.96 (m, 6H), 0.89 (m, 12H). ^{13}C NMR (100 MHz, $CDCl_3$) d: 155.10, 154.34, 153.34, 149.75, 145.15, 144.79, 140.45, 139.69, 137.14, 133.81, 133.38, 133.02, 130.03, 129.73, 128.62, 127.91, 127.38, 125.29, 122.01, 119.68, 118.44, 115.60, 68.54, 41.05, 41.00, 31.87, 30.89, 30.79, 29.96, 29.59, 26.03, 24.24, 24.19, 23.49, 22.88, 14.53, 14.30, 11.74, 11.66. MALDI: m/z calcd for [M]+, 1600.7910 (^{1}H NMR/^{13}C NMR and MALDI-TOF spectra are shown in Supporting information.

Anal. Calcd. for $C_{98}H_{116}N_6O_6S_4$ C, 73.46; H, 7.30; N, 5.25; O, 5.99; S, 8.00. Found C, 73.16; H, 7.06; N, 5.03; S, 7.84.

2.4. Photovoltaic device fabrication and characterization

The SMOSCs were fabricated with a structure of ITO/PEDOT:PSS/VC96 or VC97:$PC_{71}BM$/Al by using conventional solution spin casting technique. The indium tin oxide (ITO) coated glass substrates were cleaned sequentially by ultrasonic treatment in detergent, deionized water, acetone, and isopropyl alcohol for 20 min. A layer of PEDOT:PSS was spin coated (3500 rpm, rv35 nm thick) onto ITO glass substrate and baked at 120 oC for 20 min. The active layer was spin coated from the different weight ratios blends of VC96 or VC97 and $PC_{71}BM$ in chloroform and solvent additive (different concentration of 1,8-–diiodooctane (DIO))/chloroform solution (concentration 15 mg/mL) at 1500 rpm for 25 s on the top of ITO/PEDOT:PSS substrate. The active layer of VC96:$PC_{71}BM$ (DIO/CF) was placed on hot plate at 120 oC for 5 min, for thermal annealing treatment. Finally 60 nm Al layer was deposited onto the active layer under high vacuum by a show mask to define the active layer 20 mm^2. All devices were fabricated and tested in ambient atmosphere without encapsulation. The hole-only and electron-only devices with ITO/PEODT:PSS/active layer/Au and ITO/Al/active layer:$PC_{71}BM$/Al architectures were also fabricated in an analogous way, in order to measure the hole and electron mobility, respectively. The current–voltage characteristics of the BHJ organic solar cells were measured using a computer controlled Keithley© 238 source meter under simulated AM1.5G, 100 mW/cm^2. A xenon light source coupled with optical filter was used to give the stimulated irradiance at the surface of the devices. The incident photon to current efficiency (IPCE) of the devices was measured illuminating the device through the light source and monochromator and the resulting current was measured using a Keithley electrometer under short circuit condition (V = 0 V).

3. Results and discussion

3.1. Synthesis and characterization of VC96 and VC97

The synthesis of VC96 and VC97 is shown in Scheme 1. The molecules are based on a modular D_1-A-D_2-A-D_1 architecture. Based on this architecture the molecules VC96 and VC97 contains the donor (D_2) planar benzodithiophene, terminal donor (D_1) alkoxy triarylamine and electron deficient benzothiazole as acceptor (A). The target molecules VC96 and VC97 were achieved by a convergent synthesis strategy on the basis of Suzuki coupling and Stille coupling. Details are given in Synthesis section.

3.2. Photophysical and electrochemical properties

We start assessing the potential of the newly synthesized VC96 and VC97 small molecules for use in organic solar cells by measuring their optical properties. The UV–Visible absorption spectra of these small molecules in dilute chloroform solution and thin film are shown in Fig. 1 and corresponding optical data are summarized in Table 1. Both VC96 and VC97 show two absorption bands in the wavelength range of 300–400 nm, which can be ascribed to the p–p′ transition of the p-conjugation system [43], and another strong absorption band from wavelength region 430–650 nm (maximum absorption peak for both VC96 and VC97 538 nm) may be ascribed to the ICT transition [44] from the trithiophene moieties to the benzothiadiazole moieties, as discussed in the theoretical section. In thin film, VC97 displays a red shift k_{max} at 568 nm with a maximal absorption and also showed a vibronic shoulder around 626 nm. The VC96 film shows a broader absorption from 350 nm to 750 nm and a redshift absorption peak at 582 nm and also showed a more pronounced vibronic shoulder at 634 nm, indicating an effective p–p packing between the molecule backbones in solid state. The redshifting occurs due to the stronger intermolecular ordered packing through the planar molecular structure in thin film [45,46]. In comparison to VC97, VC96 exhibits more redshifted absorption spectrum which most likely results from enhanced planarity of VC96 chains by two conjugated alkylthiophene side chains, that suggests more efficient intermolecular p–p interaction in solid state. It is obvious that substitution of thienyl group in the side chain of BDT could effectively lower the bandgap and also improves the absorption coefficient. The optical bandgaps of VC96 and VC97, estimated from the onset absorption edge of the absorption spectrum in thin film of the small molecules, are 1.76 eV and 1.80 eV, respectively (Scheme 2).

The cyclic voltammetry (CV) was used to estimate the HOMO energy levels of these compounds (Fig. S10). The potentials were internally calibrated using the ferrocene/ferrocenium (Fc/Fc^+) of the redox couple (4.8 eV below vacuum level) [47]. The HOMO energy levels of VC96 and VC97 were estimated from the onset oxidation potential observed in CV and are −5.13 eV and −5.17 eV for VC96 and VC97, respectively (see Table 1). The HOMO energy level of VC97 is slightly deeper than that of VC96, suggesting that the VC97 ethylhexyloxy substituted BDT would be weak donor unit, lowering the HOMO level of VC97, since the weak donor unit is D-A conjugated compounds lowers the HOMO energy level. The LUMO energy level was determined using $E_{LUMO} = E_{HOMO} - E_{0-0}$. The E_{0-0} is the energy between the transition between the lowest vibrational ground state and the lowest vibrational excited state and calculated from the intersection of absorption and emission spectra of small molecules in solution (Fig. S9). The calculated LUMO energy levels of VC96 (−3.08 eV) and VC97

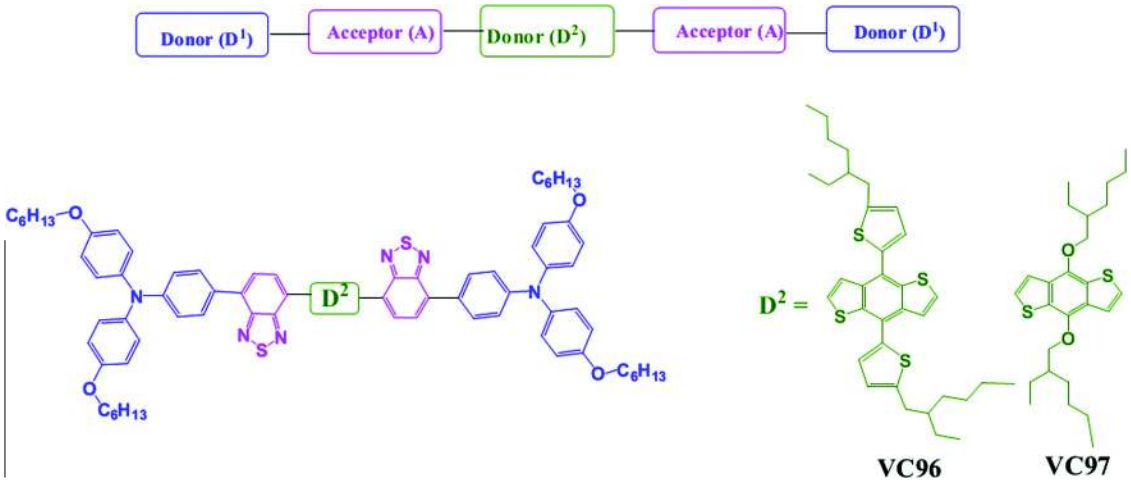

Scheme 1. Molecular structures of VC96 and VC97.

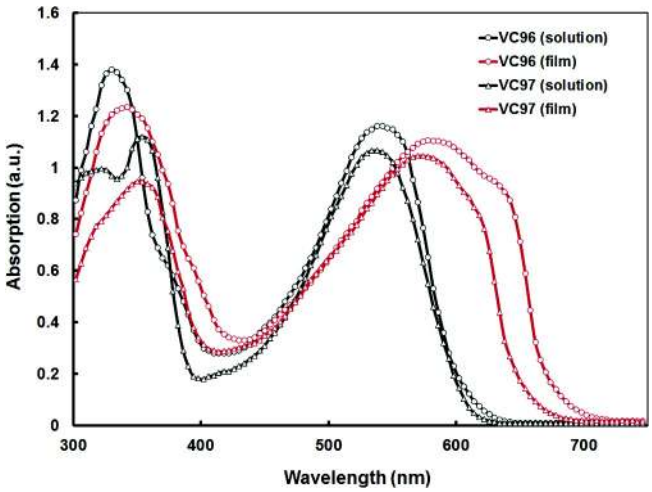

Fig. 1. Normalized absorption spectra of VC96 and VC97 in dilute chloroform solution and thin film cast from chloroform solvent.

(−3.12 eV) are 1.08 eV and 0.98 eV, respectively above the LUMO energy level of $PC_{71}BM$ (−4.1 eV) that act as electron acceptor (Fig. 2), which generates a large driving force for the transfer and separation of photogenerated charge carriers in the D-A interface.

To investigate the charge transfer from small molecules to $PC_{71}BM$, the photoluminescence (PL) spectra of VC96 and VC97 films and their corresponding blended thin films with $PC_{71}BM$ were measured and are shown in Fig. 3. Both pristine VC96 and VC97 films show a strong PL emission band with a maximum at 722 nm. However, when the small molecule is blended with $PC_{71}BM$, the emission peak of the small molecule is significantly quenched indicating an effective charge transfer from the small molecules to $PC_{71}BM$ [17]. The more pronounced quenching noted for the VC96:$PC_{71}BM$ blend compared to VC97:$PC_{71}BM$ may be a result of better interpenetrated morphology in the former blend. The PL intensity is not fully quenched indicates all the excitons generated are not dissociated and some of them are not contributing the photocurrent generation.

3.3. Theoretical calculations

We have additionally performed a theoretical study on the VC96 and VC97 molecular structures within the framework of density functional theory (DFT) and time-dependent density functional theory (TD-DFT). Details are given in Supporting information.

Vibrational analysis on the optimized structures of VC96 and VC97 did not reveal any vibrational modes with imaginary eigenfrequencies, i.e., the final optimized structures are true local (if not global) minimum. The main body of both structures is highly planar, this includes the benzodithiophene (BDT) and benzothiadiazole (BT) groups. The linking benzenes of the triphenylamine terminating groups form dihedral angles in the range of 26–33o (depending on the functional used and the presence of solvent). We have calculated the HOMO and LUMO energy levels and the optical gaps, defined here as the energetically lowest allowed vertical electronic excitation, employing the PBE, M06, and B3LYP functionals. In Table 1, in addition to the frontier orbitals' energy levels, we also provide the optical gap the main contributions to the first excitation as well as the wavelength of the first excitation and of the excitations with the largest oscillator strengths.

Table 1
Photophysical and electrochemical properties of VC96 and VC97.

Small molecules	k_{max}[a] (nm)	k_{max}[b] (nm)	k_{em} (nm)	E_{0-0}[c] (eV)	E_{ox} (V vs Fc/Fc+)[d]	E_{HOMO} (eV)	E_{LUMO}[e] (eV)	E_{gopt}[f] (eV)
VC96	539 (57,770)	582	722	2.05	0.25	−5.13	−3.08	1.76
VC97	539 (61,480)	568	720	2.05	0.29	−5.17	−3.12	1.80

[a] Measured in chloroform, in parenthesis molar extinction efficient at k_{abs} (in M^{-1} cm^{-1}).
[b] Thin film cast from chloroform.
[c] E_{0-0} was determined from the intersection of absorption and emission spectra in dilute solutions.
[d] E_{HOMO} was calculated using E_{HOMO} (vs vacuum) = −4.88 − E_{ox} (vs Fc/Fc+).
[e] E_{LUMO} was calculated using $E_{LUMO} = E_{HOMO} + E_{0-0}$.
[f] Calculated from the absorption edge in thin film.

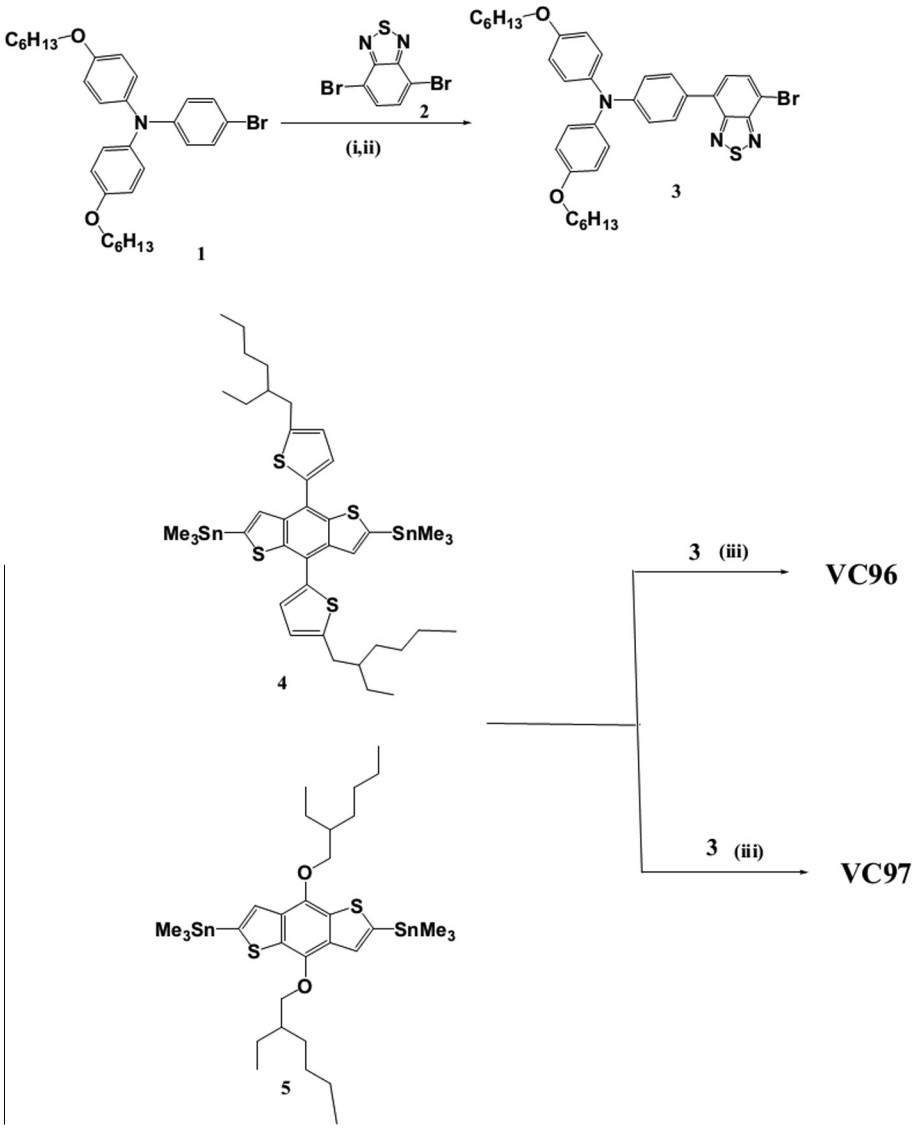

Scheme 2. Synthetic route of VC96 and VC97. Reaction conditions: (i) n-BuLi, THF, $B(OCH_3)_3$, −78 oC; (ii) $Pd(PPh_3)_4$, 2 M K_2CO_3 aqueous solution, THF, 6 h, 80 oC; (iii) Dry Toluene, $Pd(PPh_3)_4$, 110 oC, 48 h.

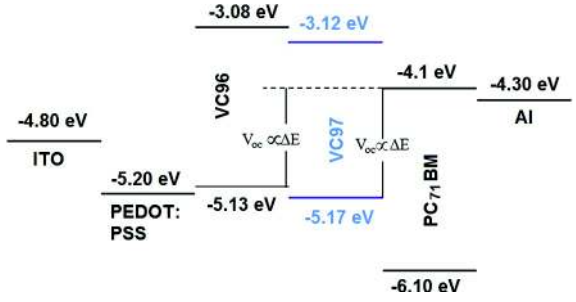

Fig. 2. HOMO and LUMO energy levels of VC96 and VC97 along with the energy levels of $PC_{71}BM$.

The HL gap calculated using the hybrid B3LYP functional is slightly smaller than that using the meta-hybrid M06 functional, however, the calculated optical gaps are practically the same for both functionals, with the later in slightly better agreement to experiment. In Table 2 we also provide the character of the first allowed excitations only for contributions larger than 4%. The first

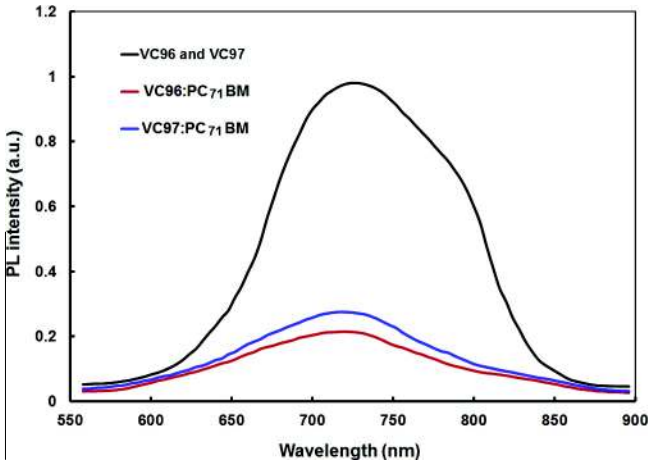

Fig. 3. PL spectra of pristine VC96, VC97 (same), VC96:$PC_{71}BM$ (1:2) and VC97:$PC_{71}BM$ (1:2) thin films cast from chloroform solvent.

Table 2
Calculated properties of VC96 and VC97.

	HOMO (eV)	LUMO (eV)	HL (eV)	OG (eV)	$k_{1st/max}$ (nm)	f	Main contributions	**1** (D)
VC96								
PBE	−4.06	−3.06	1.00					2.85
B3LYP	−4.71	−2.62	2.09	1.78	697/476/422/364/340	1.51	H→L (93%); H − 1→L + 1 (5%)	3.30
	−4.89[a]	−2.81[a]	2.07[a]	1.74[a]	712/474/431/380/368/342[a]	1.66[a]	H→L (92%); H − 1→L + 1 (6%)[a]	4.24[a]
M06	−5.03	−2.56	2.47	1.95	637/447/399/361/349/322	1.62	H→L (88%); H − 1→L + 1 (8%)	3.39
	−5.22[a]	−2.76[a]	2.46[a]	1.92[a]	646/446/403/394/350/325[a]	1.82[a]	H→L 85%; H − 1→L + 1 (9%)[a]	4.32[a]
VC97								
PBE	−3.93	−3.02	0.92					2.49
B3LYP	−4.73	−2.64	2.09	1.78	698/471/405/333/321	1.51	H→L (93%); H − 1→L + 1 (6%)	3.14
	−4.90[a]	−2.82[a]	2.08[a]	1.74[a]	711/465/411/351/337/320[a]	1.65[a]	H→L (92%); H − 1→L + 1 (7%)[a]	4.41[a]
M06	−5.05	−2.57	2.48	1.95	637/440/382/316/300	1.61	H→L (87%); H − 1→L + 1 (8%)	2.41
	−5.24[a]	−2.75[a]	2.49[a]	1.94[a]	639/434/385/321/301[a]	1.78[a]	H→L (84%); H − 1→L + 1 (11%)[a]	2.81[a]

Specifically HOMO and LUMO energies (eV), HOMO–LUMO gap (eV), HL, optical gap (eV), OG, with corresponding oscillator strengths, f, the wavelengths of the first excitation and excitations with the largest oscillator strengths, the main contributions to the first excited state, and the dipole moment (D), **1**.

[a] Values when solvent effects are taken account for chloroform.

excitation, as calculated by each of the functionals, clearly exhibits a strong single-configuration character, with only marginal secondary contributions.

In Fig. 4 we have plotted the isosurfaces (isovalue = 0.02) of the HOMO and LUMO, as well as the next nearest frontier orbitals, of the VC96 and VC97 structures. In both cases the HOMO extends over all of the main, nearly planar, body of the structures. The LUMO is delocalized mainly on the inner part of the structures, reaching up to the benzothiadiazole moieties, but not to the triphenylamine groups. We also show the HOMO − 1 and LUMO + 1 isosurfaces since transitions between them contribute to the first excitations, as shown in Table 1. For this case as well the exhibited delocalizations are different, with the HOMO − 1 mainly on the outer (triphenylamine) groups and the LUMO + 1 more inwards over the benzothiadiazole moieties. To quantify the contributions of the moieties to the frontier orbitals we have calculated the total and partial density of states (PDOS). The PDOS for VC96 and VC97 is given and discussed in Supporting information, Fig. S11. The theoretical UV–visible absorption spectra of VC96 and VC97 calculated from the B3LYP functional is also shown in Fig. S12 (Supporting information) and is closely matched with experimentally observed absorption spectra.

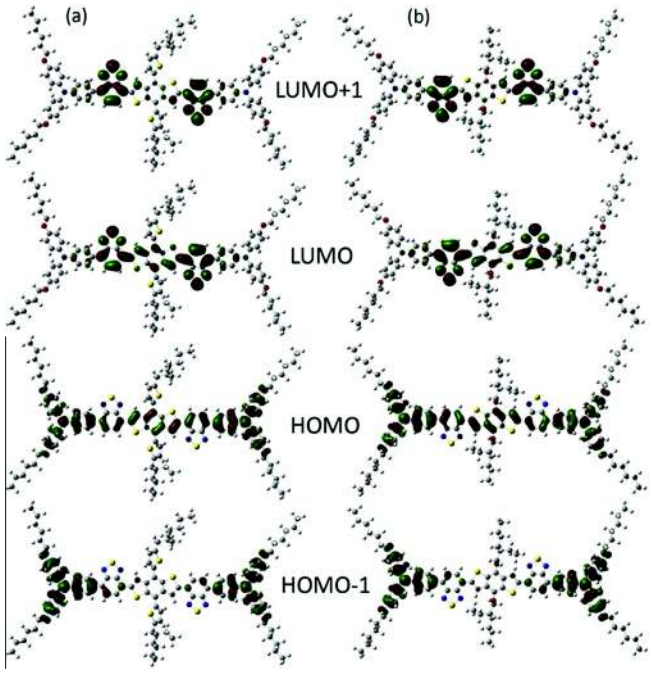

3.4. Photovoltaic properties

The photovoltaic properties of VC96 and VC97 was investigated in BHJ OSCs with a device structure ITO/PEDOT:PSS/active layer/Al. The active layer consists of donor VC96 or VC97 and $PC_{71}BM$ acceptor. It is well known that the performance of BHJOSCs could be strongly affected by the processing parameters, including the small molecule/$PC_{71}BM$ ratio (w/w) and thicknesses of active layer. The OSC performance was first optimized by processing donor (VC96 or VC97:$PC_{71}BM$ (1:2 by weight) with thickness of 90 nm BHJ thin film from CF solution. We have fabricated 8 devices and presented the results of best device. The current–voltage characteristics of the device were shown in Fig. 5a and the resulted photovoltaic parameters are summarized in Table 3. The VC96 showed a PCE of 4.06% with a J_{sc} of 8.36 mA/cm^2, V_{oc} of 0.90 V and FF of 0.54. The VC97 showed a PCE of 3.12% with J_{sc} of 6.78 mA/cm^2, V_{oc} of 0.92 V and FF of 0.50. The slightly higher V_{oc} for VC97 based OSCs was observed, in comparison with that of VC96. The origin of slight enhancement in V_{oc} for VC97 based device may be attributed to the deeper HOMO energy level of VC97 (−5.17 eV) as compared to VC96 (−5.13 eV), due to the weak electron donating ability of ethylhexyloxy substituted BDT unit in VC97. Since V_{oc} of BHJ organic solar cells is proportional to the difference in the HOMO energy level of electron donor and LUMO of electron acceptor, the slightly larger energy offset between VC97 and $PC_{71}BM$ lead to an enhanced V_{oc} from the OSCs.

The enhancement in the PCE of VC96 based device as compared to VC97 is due to the higher values of J_{sc} and FF. We have estimated the shunt resistance (R_{sh}) derived from the from the J–V characteristics in dark (as shown in Fig. 6) and fitting with the well known diode Shockley [48]. The R_s and R_{sh} of the devices are complied in Table 3. The smaller R_s indicate that there is a favorable charge transport within OSCs. On the other, larger R_{sh} indicates that the reverse current density (originated from the recombination of electron and hole during their transportation through active layer towards the respective collecting electrodes) is smaller resulting higher FF. Therefore, the enhancement in the FF for the device based on VC96 as compared to VC97 may be better charge transport and reduced charge recombination in the VC96 based device.

We have investigated the incident photon to current conversion efficiency (IPCE) spectra of the devices and shown in Fig. 5b. As shown in Fig. 5b, the IPCE spectra of VC96:$PC_{71}BM$ and

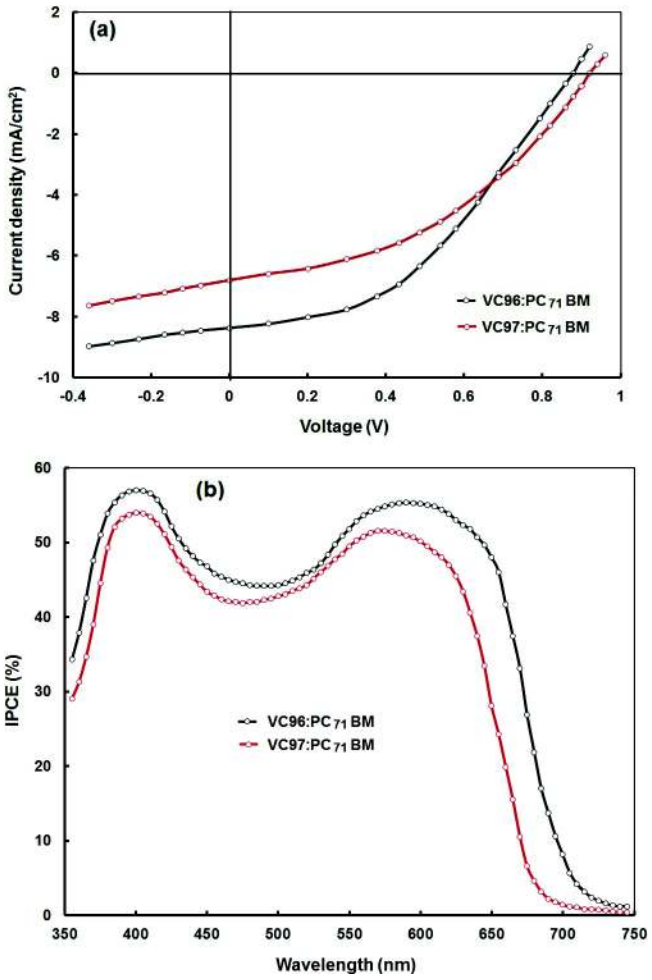

Fig. 5. (a) Current–voltage (J–V) under illumination (AM1.5100 mW/cm^2) and IPCE spectra of the OSCs based on VC96:$PC_{71}BM$ (1:2) and VC97:$PC_{71}BM$ (1:2) films processed from chloroform solvent.

spectral properties of VC96 and VC97 thin films. The VC96:$PC_{71}BM$ based OSC exhibits a broad and high response region, covering from 350 to 700 nm, while the VC97:$PC_{71}BM$ based OSC exhibits a relatively narrower and lower response covering from 350 to 680 nm, which is in good agreement with UV–Vis absorption of VC96 and VC97 thin film as shown in Fig. 1a and b (red color). The J_{sc} estimated from the integration of IPCE spectra are 8.25 mA/cm^2 and 6.62 mA/cm^2 for VC96 and VC97 based OSCs, respectively, implying that the wider absorption band of VC96 relative to VC97 indeed contributes to the light harvesting. The larger value of J_{sc} and PCE for the device with VC96 is caused by its broader absorption spectrum in thin film and higher hole mobility by introducing the conjugated side chain [30]. The improved value of J_{sc} and PCE for the device based on VC96:$PC_{71}BM$ as compared to VC97:$PC_{71}BM$ also get support from the PL spectra of these blends (Fig. 3), in which the PL quenching is more effective for former than later blend.

The morphology and crystallinity of the active layer is the deciding factor of charge transport and J_{sc} of the OSCs. We have recorded the X-ray diffraction pattern (XRD) of the pristine and blended layer. To record the XRD pattern, the films were cast from the chloroform on the Si substrates under the optimized device fabrication conditions with same concentration and weight ratio. The XRD pattern for pristine VC96 and VC97 are shown in Fig. 7a. The XRD pattern of pristine film illustrates that the both VC96 and VC97 have significant (1 0 0) diffraction peaks at $2h = 4.82^o$ and $2h = 3.96^o$, respectively, which results from the chain packing with corresponding d spacing of 18 Å and 22.8 Å, respectively. The difference in the d-spacing may resulted from different substituted units attached to the BDT core and small d-spacing indicating a denser packing for VC96. XRD data illustrates that VC96 possesses higher degree of crystallinity than VC97. The d-spacing and p–p stacking distance corresponds to the main diffraction peaks of VC96 are both smaller than for VC97 film. The short p–p stacking distance of VC96 indicates that chains are more likely to form a planar conformation in the solid film, resulting in a redshift in the absorption spectrum, which is good agreement with the absorption of VC96 in thin film. The planarity of main chain and short p–p stacking distance would facilitate charge transport, resulting in higher hole mobility. The diffraction peaks of the blended films were identical to those of corresponding pristine films (Fig. 7b), which suggests a more compact packing of VC96 in the blend. Moreover, the width of half peak of the (1 0 0) of VC96 is narrower than that of VC97, which indicates that VC96 has better ordered crystalline domains in the blend than VC97 and it is easier for $PC_{71}BM$ to admix into the loosely stacked VC97 molecules than VC96. This ease of insertion results in higher miscibility of VC97 and $PC_{71}BM$, which has adverse effects on the purity of the crystalline domains [49–51], and thus leads to widening of the half peak of the (1 0 0). In the case of VC96:$PC_{71}BM$ blend the well ordered crystalline domains of the VC96 donor promote the escape of charge from the D-A interface, which reduces the bimolecular recombination, a higher utilization rate of absorbed photons and a higher J_{sc}.

Both small molecules have same chemical structure expect for the central BDT core. In order to obtain information about the influence of different substitution at the side chain of the BDT core on their transport properties, hole mobilities (μ_h) of the hole only devices were measured by space charge limited current (SCLC) with a device ITO/PEDOT:PSS/active layer/Au. The SCLC is estimated by the Mott–Gurney equation, i.e., $J = 9\varepsilon_o\varepsilon_r\mu_h V^2/L^3$, in which J is the current density, L is the film thickness (90 nm), μ is the hole mobility, ε_r is the relative dielectric constant of the transporting

Table 3
Photovoltaic parameters for the optimized BHJ devices.

Blend	J_{sc} (mA/cm^2)	V_{oc} (V)	FF	PCE (%)	R_s (X cm^2)	R_{sh} (X cm^2)	μ_h (cm^2/Vs)	μ_e (cm^2/Vs)	μ_e/μ_h
VC96:$PC_{71}BM$[a]	8.36	0.90	0.54	4.06 (3.98)*	31.6	724	2.34×10^{-5}	2.56×10^{-4}	10.94
VC97:$PC_{71}BM$[a]	6.78	0.92	0.50	3.12 (3.06)*	38.4	687	9.72×10^{-6}	2.45×10^{-4}	25.20
VC96:$PC_{71}BM$[b]	10.72	0.86	0.59	5.44 (5.38)*	24.4	937	6.78×10^{-5}	2.42×10^{-4}	3.57
VC97:$PC_{71}BM$[b]	9.42	0.88	0.56	4.64 (4.56)*	24.6	813	3.45×10^{-5}	2.38×10^{-4}	6.90
VC96:$PC_{71}BM$[c]	11.42	0.88	0.61	6.13 (6.05)*	12.4	1045	8.87×10^{-5}	2.40×10^{-4}	2.70

[a] CF cast.
[b] DIO (4 v%)/CF cast.
[c] DIO/(4 v%)/CF and subsequent thermal annealing.
* Average of 8 devices.

Fig. 4. Frontier and near frontier orbitals of (a) VC96, and (b) VC97.

VC97:$PC_{71}BM$ based OSCs are consistent with the absorption

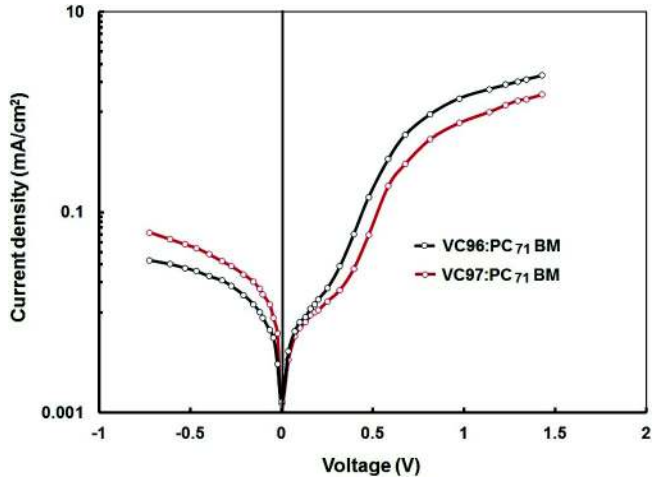

Fig. 6. Current–voltage (J–V) characteristics (dark) in semilog plot VC96:$PC_{71}BM$ and VC97:$PC_{71}BM$ based devices.

medium, e_o is the permittivity of free space (8.85×10^{-12} F/m), V is the internal voltage of the device, derived as $V = V_{app} - V_{bi}$, where V_{app} is the applied voltage and V_{bi} is the built in voltage due to the relative work function difference of the two electrodes. Fig. 8 shows the J–V characteristics of optimized hole only devices using VC96:$PC_{71}BM$ and VC97:$PC_{71}BM$ active layers, in dark. The hole mobility estimated from the Fig. 8 and fitting with the Mott-Gurney equation are 2.34×10^{-5} and 9.72×10^{-6} cm^2/Vs for VC96 and VC97, respectively. Hole mobility is determined by intramolecular backbone and intermolecular packing. Both the small molecules have the same end capping unit and p-bridges, therefore the difference in the mobilities may probably depend on the intermolecular packing induced by the different central BDT donor core. It is obvious that VC96 that exhibits a relative higher hole mobility than VC97 may be attributed to more an effective intermolecular packing triggered by its BDT segment with

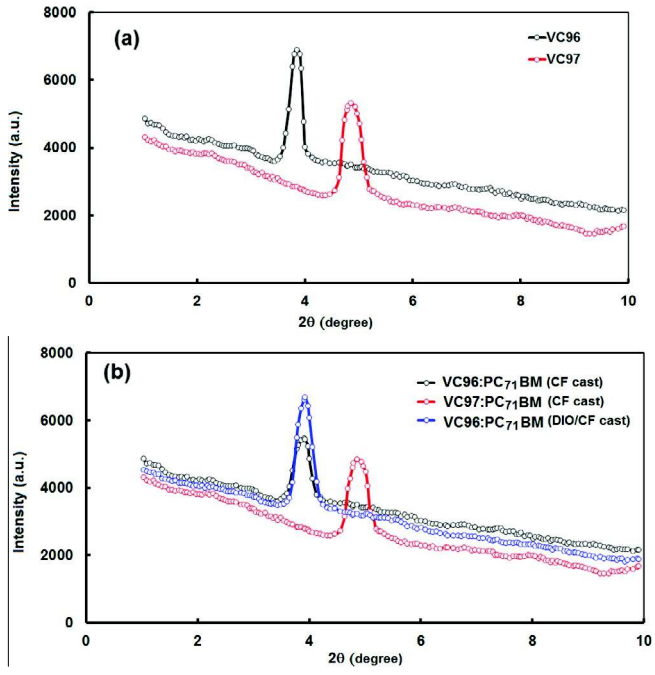

Fig. 7. XRD patterns of (a) pristine VC96 and VC97 and (b) VC96:$PC_{71}BM$ (CF cast), VC97:$PC_{71}BM$ (CF cast) and VC96:$PC_{71}BM$ (DIO/CF cast).

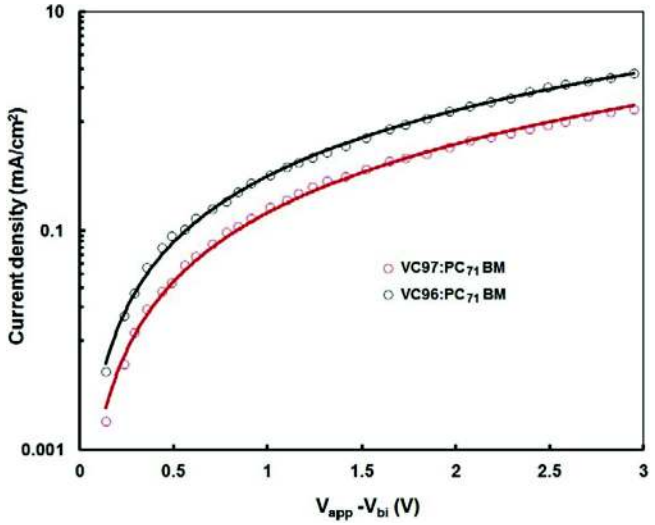

Fig. 8. J–V characteristics of hole only devices processed with CF solvent, solid line are SCLC fitted.

ethylhexyl-thiophene side unit. In comparison to VC97, VC96 showed a stronger intermolecular interaction as evidenced by the more red-shifted absorption in thin film, contributing to its charge carrier transporting ability [52–56], which is also responsible for higher FF and J_{sc} of VC96 based device. This also verifies that introduction of two dimensional moiety with p-stacking can increase hole mobility due to better molecular packing [57,58]. The low mobility of VC97 indicates that charges were not extracted efficiently prior to recombination from mutual columbic attraction, resulting in low values of FF and J_{sc} [59].

The PCE of devices using either VC96 or VC97 as donor along with $PC_{71}BM$ as acceptor is low compared to the polymer and small molecules investigated so far. Since in our devices, the V_{oc} of both devices is quite high and reasonably comparable to other devices based on similar small molecules, therefore, the low value of PCE is mainly due to the low values of J_{sc} and FF. This may be attributed to insufficient exciton generation and their dissociation and also poor charge transportation and collection as evidenced from the PL spectra. It is reported that optimal BHJ morphologies consist of robust bicontinuous nanoscale domains of each donor and acceptor components on the order of exciton diffusion length, which extend vertically from each electrode, thereby increasing the surface area of domains and forming continuous conducting pathways for efficient charge extraction and transport, is necessary [60]. An optimal morphology can be achieved during film formation, therefore, a number of processing techniques such as thermal and solvent annealing, have been explored to control the blend morphology [61,62]. Besides these processing techniques, solvent additive (SA) processing is a commonly used method for the deposition of BHJ active layers for high performing solar cells based on conjugated polymer solar cells [63,64] and small molecules [65–68]. This technique relies on the addition of a small amount of a high boiling point solvent to the host solvent and has an impact on the solar cell parameters, such as J_{sc}, V_{oc}, FF and ultimately PCE. The SA (solvent additive) has shown to modify the internal order with phases and can increase the crystallinity of conjugated polymers [69–71]. In an effort to improve the performance of the BHJ organic solar cell based on these small molecules, we have used SA method and prepared the active layer with different concentrations of DIO as SA (1%, 2%, 3% and 4% v) and tested them for both VC96:$PC_{71}BM$ and VC97:$PC_{71}BM$ blends and found 3% v to be the optimized concentration. The current voltage characteristics of the resulting devices are shown in Fig. 9a and the corresponding

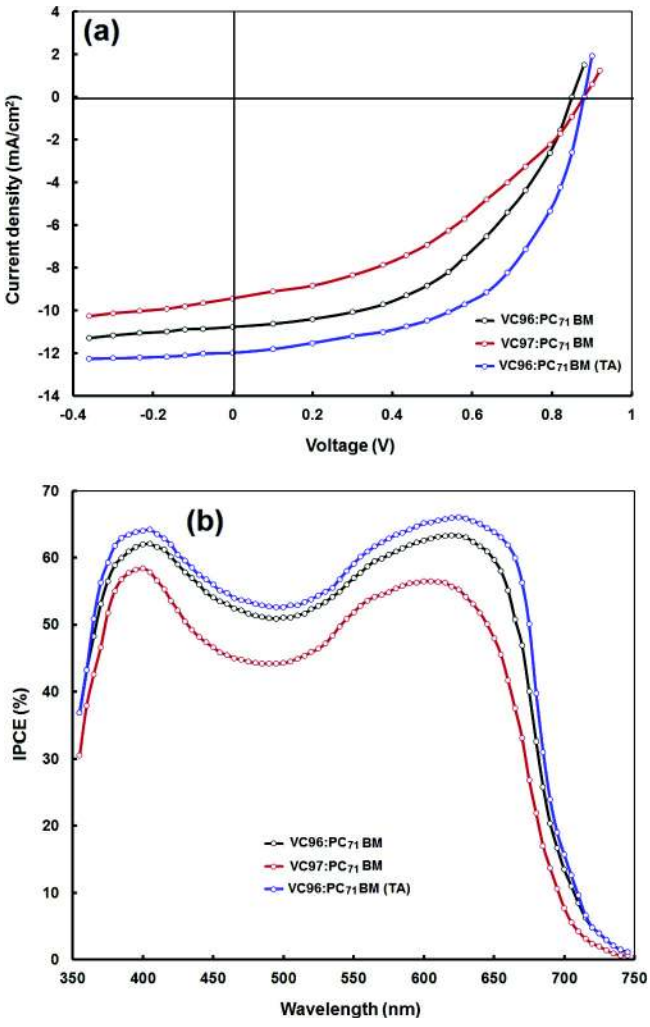

Fig. 9. (a) Current–voltage (J–V) under illumination (AM1.5100 mW/cm^2) and IPCE spectra of the OSCs based on VC96:PC_{71}BM (1:2) and VC97:PC_{71}BM (1:2) films processed from DIO (3 v%)/chloroform solvent.

photovoltaic parameters are complied in Table 3. Remarkably, the PCE of the device was improved up to 5.44% (J_{sc} = 10.72 mA/cm^2, V_{oc} = 0.86 V and FF = 0.59) and 4.72% (J_{sc} = 9.42 mA/cm^2, V_{oc} = 0.88 V and FF = 0.57) for VC96:PC_{71}BM and VC97:PC_{71}BM based devices, respectively. We have also used the thermal annealed solvent additive (TASA) VC96:PC_{71}BM as active layer and the PCE of the device was improved up to 6.13% (J_{sc} = 11.42 mA/cm^2, V_{oc} = 0.88 V and FF = 0.61).

The increase in the PCE of the devices, upon SA and TASA, UV–Vis absorption spectra of the blend films and IPCE spectra were measured. As shown in Fig. 10, in comparison to the spectra of CF cast blended films, the spectra of the film cast from SA, the absorption peak corresponds to the ICT band are redshifted, which is related to enhanced p–p stacking. For TASA treatment, the absorption intensity was overall improved, thus resulting enhanced exciton generation and thereby J_{sc}. As can be seen from IPCE spectra (Fig. 9b), uniform increase of the spectral response across the whole wavelength region, are clearly observed for the devices with SA blends. Furthermore, for the device based on TASA, the IPCE was improved again in whole wavelength region, which indicates that exciton generation and subsequent dissociation into charge carrier and their transportation through the active layer were simultaneously enhanced. The calculated values of J_{sc} from the integration of IPCE are 10.67 mA/cm^2, 9.34 mA/cm^2 and 11.32 mA/cm^2 for VC96:PC_{71}BM (SA), VC97:PC_{71}BM (SA) and VC96:PC_{71}BM (TASA), respectively, which is consistent with the J_{sc} value obtained from J–V characteristics.

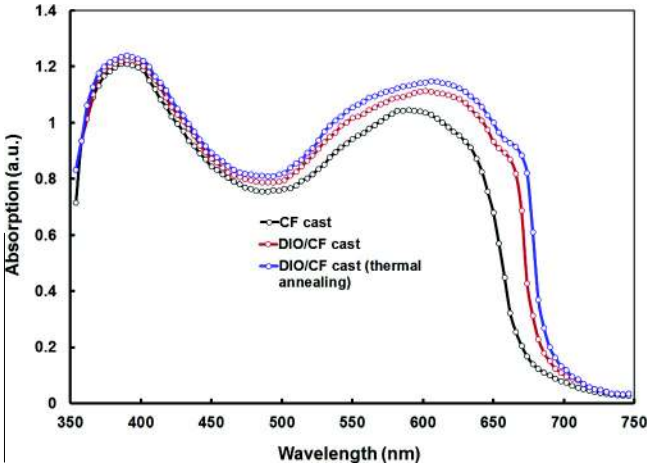

Fig. 10. Absorption spectra of VC96:PC_{71}BM (1:2) thin films cast in different conditions.

The morphology of the active layer plays an important role in the exciton dissociation and charge transport within the active layer. Therefore, atomic force microscopy (AFM) and transmission electron microscopy (TEM) were used to investigate the effect of different treatment on the morphology of the blended thin films (shown only for VC96:PC_{71}BM blend thin films). The AFM images of the VC96:PC_{71}BM processed in different conditions are shown in Fig. 11. The root mean squared (rms) surface roughness of the blend films prepared with and without SA are 2.24 and 2.96 nm, respectively. The decrease rms could be attributed to the more dispersive PC_{71}BM domains induced by the DIO additive and further decreased up to 1.52 nm with SATA treatment. The further decrease in the rms value, indicating that the aggregation levels of VC96 domains was decreased. Fig. 12 shows the TEM images of VC96:PC_{71}BM thin films. Compared to the film cast from CF, better phase separations have been achieved for SA and TASA an even better phase separation was observed. The more homogeneous D-A distribution in the active layer is beneficial for exciton dissociation and charge carrier transport as well their balance in the active layer [72,73].

In order to further demonstrate that the simultaneous improved charge transport ability and their balance in the active layer, we have measured the hole mobility in the active layer, processed with different treatment, from the J–V characteristics of the hole only devices in dark (Fig. 13) and using SCLC model. For the SA based devices, the hole mobility increased up to 6.78 x 10^{-5} cm^2/Vs and 3.45 x 10^{-5} cm^2/Vs for VC96:PC_{71}BM and VC97:PC_{71}BM, respectively. Additionally, the device based on TASA processed VC96:PC_{71}BM exhibits a higher hole mobility (8.87 x 10^{-5} cm^2/Vs) and with much more balanced charge transport as shown in Table 3. The balanced charge transport is beneficial for improved FF.

The improved PCE of the devices with SA and TASA processed active layers are supported by the relation of photocurrent density (J_{ph}) versus effective voltage (V_{eff}). $J_{ph} = J_L - J_D$, where J_L and J_D are the current densities under illumination and in dark, respectively. $V_{eff} = V_o - V_{app}$, V_o is the voltage at which $J_{ph} = 0$ and V_{app} is applied voltage [74,75]. A plot of J_{ph} vs V_{eff} for VC96:PC_{71B}M based devices, processed in different conditions is shown in Fig. 14. In the case of VC96:PC_{71}BM cast from CF solvent, the J_{ph} shows a stronger field dependence across the large bias range and has not fully saturate even V_{eff} ~ 3.5 V, suggesting a significant germinate and/or

Fig. 4. Frontier and near frontier orbitals of (a) VC96 and (b) VC97.

VC97:PC_{71}BM based OSCs are consistent with the absorption

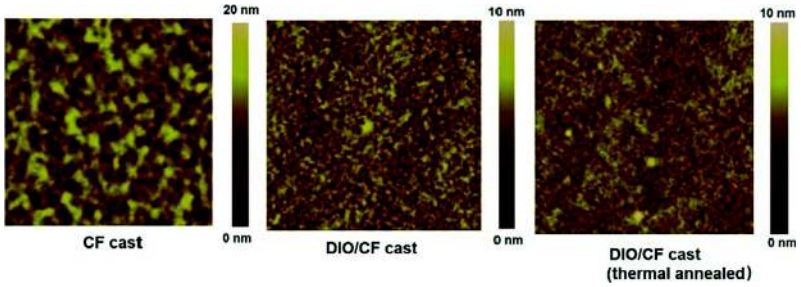

Fig. 11. AFM images of VC96:$PC_{71}BM$ thin films cast in different conditions.

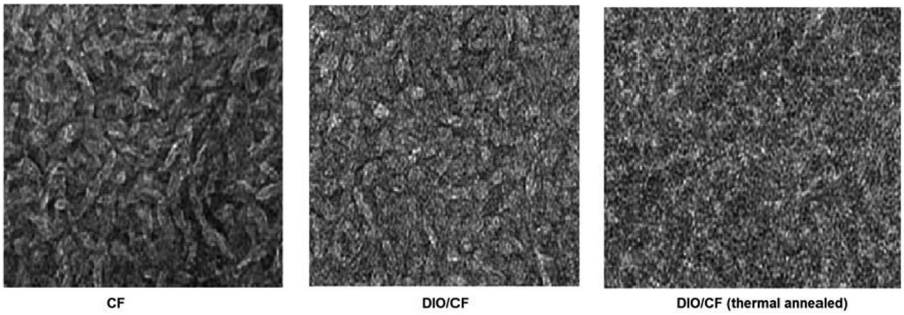

Fig. 12. TEM images of VC96:$PC_{71}BM$ thin films cast in different conditions.

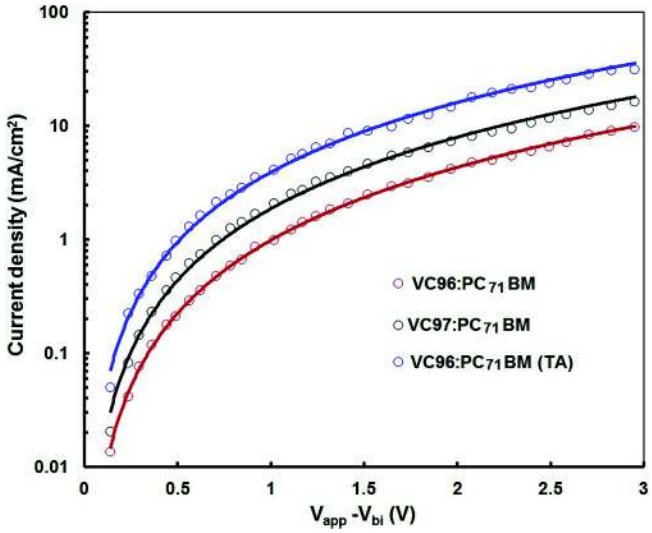

Fig. 13. J–V characteristics of hole only devices processed with DIO/CF solvent, solid line are SCLC fitted.

bimolecular recombination and less efficient charge collection at the electrodes, thus a lower FF [76]. However, the device processed with SA and TASA, J_{ph} has a linearly dependence on voltage at the low value of V_{eff}, and J_{ph} reaches saturation, when the effective voltage reaches to 2.4 V and 2.0 V, respectively. This suggest that the photogenerated excitons are dissociated into free charge carriers and charge carriers are collected at the electrodes efficiently with reduced bimolecular recombination for the devices based on blends processed with SA and TASA treatment. The ratio of J_{ph}/J_{sat} under short circuit conditions gives information about the overall exciton dissociation and charge collection efficiency [77]. Under short circuit conditions, the ratios are 0.69, 0.81 and 0.84 for VC96:$PC_{71}BM$ (CF cast), VC96:$PC_{71}BM$ (DIO/CF cast), thermally annealed VC96:$PC_{71}BM$ (DIO/CF cast) based devices, respectively.

The exciton dissociation and charge transport is more efficient in the device based on blend processed with TASA as compared to SA, due to the better nanoscale morphology and interpenetrating network pathways for exciton dissociation and charge transportation, respectively. Moreover, the devices based on DIO/CF processed films have larger shunt resistance than CF cast and even higher for thermally annealed DIO/CF, while they exhibit smaller series resistance than that of CF cast (as shown in Table 3), indicating that better ohmic contact is formed for SA and TASA processed films. These results indicates that in CF processed active layer based devices, the space charge in build up and bimolecular recombination are dominating, but the devices based on SA and TASA processed active layer, these effects are reduced substantially due the more balanced charge transport as indicated by the increased hole mobility. Moreover, the variation of J_{sc} as a function

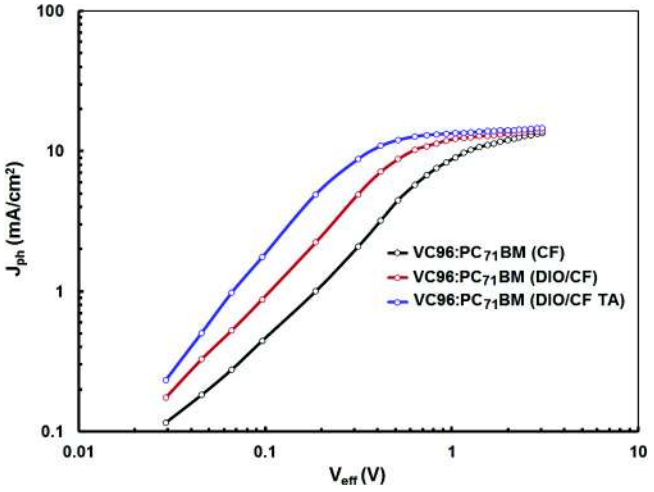

Fig. 14. Photocurrent density (J_{ph}) versus effective voltage (V_{eff}) characteristics for devices based on VC96:$PC_{71}BM$ processed under different conditions under constant incident light intensity.

of light intensity (P_{in}) showed a power law dependence, i.e., $J_{sc} \nearrow (P_{in})^{a}$. The values of exponent a are 0.86, 0.92 and 0.94 for CF cast, SA and TASA processed film based devices, respectively, indicating a lesser bimolecular recombination in the latter devices as compared to CF cast.

4. Conclusions

In summary, we have designed and synthesized two D_1-A-D_2-A-D_1 small molecules with same D_1, A, and different core donor (D_2) denoted as VC96 and VC97 and investigated their optical and electrochemical properties for their potential application as donor in bulk heterojunction solar cells. The solution processed BHJ small molecule processed with CF solution showed PCE of 4.06% and 3.12% for VC96:PC_{71}BM and VC97:PC_{71}BM active layers, respectively. The higher PCE of device based on the former active layer than that of latter is attributed to the broader absorption profile of VC96 and larger hole mobility. In an attempt to improve the PCE, we have the adopted solvent additive (SA), i.e., 3% v DIO/CF technique and achieved PCE of 5.44% and 4.72%, for VC96:PC_{71}BM and VC97:PC_{71}BM active layer, respectively. The PCE has been further improved up to 6.13%, when DIO/CF processed VC96:PC_{71}BM was thermally annealed at 110 oC for 10 min. The enhancement in the PCE with SA and thermally annealed SA based device is attributed to the balanced charge transport, higher light harvesting ability, and better nanoscale morphology for exciton dissociation and charge transport and collection, supported by the, PL, AFM, TEM and mobility results.

Acknowledgements

We would like to thank MINECO for the Project CTQ2013-47183-R and the support through Severo Ochoa Excellence Accreditation 2014–2018 (SEV-2013-0319). We are also thankful to Material Science laboratory, MNIT, Jaipur for the availability of device fabrication facilities and other characterization.

Appendix A. Supplementary data

Supplementary data associated with this article can be found, in the online version, at http://dx.doi.org/10.1016/j.orgel.2015.07.014.

References

[1] F.C. Krebs, Fabrication and processing of polymer solar cells, Sol. Energy Mater. Sol. Cells 93 (2009) 394–412.
[2] A.C. Arias, J.D. Mackenzie, I. McCulloch, J. Rivnay, A. Salleo, Materials and applications for large area electronics: solution-based approach, Chem. Rev. 110 (2010) 3–24.
[3] M. Helgesen, R. Søndergaard, F.C. Krebs, Advanced materials and processes for polymer solar cells, J. Mater. Chem. 20 (2010) 36–60.
[4] G. Yu, J. Gao, J.C. Hummelen, F. Wudl, A.J. Heeger, Polymer photovoltaic cells: enhanced efficiencies via a network of internal donor–acceptor heterojunctions, Science 270 (1995) 1789–1791.
[5] B.C. Thompson, J.M.J. Frechet, Polymer: fullerene composite solar cells, Angew. Chem., Int. Ed. 47 (2008) 58–77.
[6] Z. He, S. Su, M. Xu, H. Wu, Y. Cao, Enhanced power conversion efficiency in polymer solar cells using an inverted device structure, Nat. Photonics 6 (2012) 591–595.
[7] S. Liao, J. Huo, Y. Cheng, S. Chen, Fullerene derivative doped zinc–oxide nanofilm as the cathode of inverted polymer solar cells with low bandgap polymer (PTB7-Th) for high performance, Adv. Mater. 25 (2013) 4766–4771.
[8] L. Dou, J. You, Z. Hong, Z. Xu, G. Li, R.A. Street, Y. Yang, 25th anniversary article: a decade of organic/polymeric photovoltaic research, Adv. Mater. 25 (2013) 6642–6671.
[9] X. Guo, N. Zhou, S.J. Lou, J. Smith, D. Tice, J. Hennek, R. Ponce Ortiz, J. Lopez Navarrete, S. Li, J. Strzalka, L. Chen, R. Chang, A. Facchetti, T.J. Marks, Polymer solar cells with enhanced fill factors, Nat. Photonics 7 (2013) 825–833.
[10] J. Roncali, Molecular bulk heterojunctions: an emerging approach to organic solar cells, Acc. Chem. Res. 42 (2009) 1719–1730.
[11] B. Walker, C. Kim, T.Q. Nguyen, Small molecule solution processed bulk heterojunction solar cells, Chem. Mater. 23 (2011) 470–482.
[12] Y. Sun, G.C. Welch, W.L. Leong, C.J. Takacs, G.C. Bazan, A.J. Heeger, Solution processed small molecule solar cells with 6% efficiency, Nat. Mater. 11 (2012) 44–48.
[13] N. Lim, N.N. Cho, S. Paek, C. Kim, J.K. Lee, J. Ko, High performance organic solar cells with efficient semiconducting small molecules containing an electron rich benzodithiophene derivative, Chem. Mater. 26 (2014) 2283–2288.
[14] A. Mishra, P. Bäuerle, Small molecule organic semiconductors on the move: promises for future solar energy technology, Angew. Chem., Int. Ed. 51 (2012) 2020–2067.
[15] Y. Lin, Y. Li, X. Zhan, Small molecule semiconductors for high efficiency organic photovoltaics, Chem. Soc. Rev. 41 (2012) 4245–4272.
[16] J.E. Coughlin, Z.B. Henson, G.C. Welch, G.C. Bazan, Design and synthesis of molecular donors for solution processed high efficiency organic solar cells, Acc. Chem. Res. 47 (2014) 257–270.
[17] A.K.K. Kyaw, D.H. Wang, D. Wynands, J. Zhang, T.Q. Nguyen, G.C. Bazan, A.J. Heeger, Improved light harvesting and improved efficiency by insertion of an optical spacer (ZnO) in solution processed small molecule solar cells, Nano Lett. 13 (2013) 3796–3801.
[18] J. Zhou, Y. Zuo, X. Wan, G. Long, Q. Zhang, W. Ni, Y. Liu, Z. Li, G. He, C. Li, B. Kan, M. Li, Y. Chen, Solution processed and high-performance organic solar cells using small molecules with a benzodithiophene unit, J. Am. Chem. Soc. 135 (135) (2013) 8484–8487.
[19] B. Kan, Q. Zhang, M. Li, X. Wan, W. Ni, G. Long, Y. Wang, X. Yang, H. Feng, Y. Chen, Solution processed organic solar cells based on dialkylthiol-substituted benzodithiophene unit with efficiency near 10%, J. Am. Chem. Soc. 136 (2014) 15529–15532.
[20] J. Zhou, X. Wan, Y. Liu, Y. Zuo, Z. Li, G. He, G. Long, W. Ni, C. Li, X. Su, Y. Chen, Small molecule based on benzo[1,2-b:4,5-b′]dithiophene unit for high performance solution processed organic solar cells, J. Am. Chem. Soc. 134 (2012) 16345–16351.
[21] Q. Zhang, B. Kan, F. Liu, G. Long, X. Wan, X. Chen, Y. Zuo, W. Ni, H. Zhang, M. Li, Z. Hu, F. Huang, Y. Cao, Z. Liang, M. Zhang, T.P. Russell, Y. Chen, Small molecule solar cells with efficiency over 9%, Nat. Photon. 9 (2015) 35–41.
[22] B. Kan, M. Li, Q. Zhang, F. Liu, X. Wan, J. Wang, W. Ni, G. Long, X. Yang, H. Feng, Y. Zuo, M. Zhang, F. Huang, Y. Cao, T.P. Russell, Y.A. Chen, Series of simple oligomer-like small molecules based on oligothiophenes for solution processed solar cells with high efficiency, J. Am. Chem. Soc. 137 (2015) 3886–3893.
[23] Y. Liu, C. Chen, Z. Hong, J. Gao, Y. Yang, H. Zhou, L. Dou, G. Li, Y. Yang, Solution processed small molecule solar cells: breaking the 10% power conversion efficiency, Sci. Rep. 3 (2013) 3356.
[24] Heliatek, Heliatek consolidates its technology leadership by establishing a new world record for organic solar technology with a cell efficiency of 12%, available at: <http://www.heliatek.com/wp-content/uploads/2013/01/130116_PR_Heliatek_achieves> record cell efficiency for OPV.pdf. (January, 2013).
[25] J. Liu, Y. Sun, P. Moonsin, M. Kuik, C.M. Proctor, J. Lin, B.B. Hsu, Tri-diketopyrrolopyrrole molecular donor materials for high performance solution processed bulk heterojunction solar cells, Adv. Mater. 25 (2013) 5898–5903.
[26] D. Patra, T.Y. Huang, C.C. Chiang, R.O.V. Maturana, C.W. Pao, K.C. Ho, K.H. Wei, C.W. Chu, 2-Alkyl-5-thienyl-substituted benzo[1,2-b:4,5-b′]dithiophene based donor molecules for solution processed organic solar cells, ACS Appl. Mater. Interfaces 5 (2013) 9494–9500.
[27] L. Huo, J. Hou, S. Zhang, H.Y. Chen, Y.A. Yang, A polybenzo[1,2-b:4,5-b′]dithiophene derivative with deep HOMO level and its application in high performance polymer solar cells, Angew. Chem., Int. Ed. 49 (2010) 1500–1503.
[28] M. Li, W. Ni, X. Wan, Q. Zhang, B. Kan, Y. Chen, Benzo[1,2-b:4,5-b′]dithiophene (BDT) based small molecules for solution processed organic solar cells, J. Mater. Chem. A 3 (2015) 4765–4776.
[29] J. Huang, C. Zhan, X. Zhang, Y. Zhao, Z. Lu, H. Jia, B. Jiang, J. Ye, S. Zhang, A. Tang, Y. Liu, Q. Pei, Y. Yao, Solution processed DPP-based small molecule that gives high photovoltaic efficiency with judicious device optimization, ACS Appl. Mater. Interfaces 5 (2013) 2033–2039.
[30] S. Shen, P. Jiang, C. He, J. Zhang, P. Shen, Y. Zhang, Y. Yi, Z. Zhang, Z. Li, Y. Li, Solution processable organic molecule photovoltaic materials with bithienyl-benzodithiophene central unit and indenedione end groups, Chem. Mater. 25 (2013) 2274–2281.
[31] Y. Lin, L. Ma, Y. Li, Y. Liu, D. Zhu, X. Zhan, A solution processable small molecule based on benzodithiophene and diketopyrrolopyrrole for high performance organic solar cells, Adv. Energy Mater. 3 (2013) 1166–1170.
[32] Z. Du, Y. Chen, W. Chen, S. Qiao, S. Wen, Q. Liu, D. Zhu, M. Sun, R. Yang, Development of new two-dimensional small molecules based on benzodifuran for efficient organic solar cells, Chem. Asian J. 9 (2014) 2621–2627.
[33] H. Zhou, L. Lang, S.C. Price, K.J. Knight, W. You, Enhanced photovoltaic performance of low bandgap polymers with deep LUMO levels, Angew. Chem., Int. Ed. 49 (2010) 7992–7995.
[34] H. Zhou, L. Yang, S. Stoneking, W. You, A weak donor–strong acceptor strategy to design ideal polymers for organic solar cells, ACS Appl. Mater. Interfaces 2 (2010) 1377–1383.
[35] H.M. Ko, H. Choi, S. Paek, K. Kim, K. Song, J.K. Lee, J. Ko, Molecular engineering of push pull chromophore for efficient bulk heterojunction morphology in solution processed small molecules organic photovoltaic, J. Mater. Chem. 21 (2011) 7248–7253.

[36] H. Choi, S. Paek, J. Song, C. Kim, N. Cho, J. Ko, Synthesis of annulated thiophene perylene bisimide analogues: their applications to bulk heterojunction organic solar cells, Chem. Commun. 47 (2011) 5509–5511.

[37] J. Lee, M.H. Yun, J. Kim, J.Y. Kim, C. Yang, Towards the realization of a practical diketopyrrolopyrrole based small molecule for improved efficiency in ternary BHJ solar cells, Macromol. Rapid Commun. 33 (2012) 140–145.

[38] P. Dutta, J. Kim, S.H. Eom, W.H. Lee, I.N. Kang, S.H. Lee, An easily accessible donor–p–acceptor conjugated small molecule from a 4,8-dialkoxybenzo[1,2-b:4,5-b$^{\prime}$]dithiophene unit for efficient solution processed organic solar cells, ACS Appl. Mater. Interfaces 4 (2012) 6669–6675.

[39] Y. Shirota, H. Kageyama, Charge carrier transporting molecular materials and their applications in devices, Chem. Rev. 107 (2007) 953–1010.

[40] C. He, Q.G. He, Y.P. Yi, G.L. Wu, F.L. Bai, Z.G. Shuai, G. Shuai, Y.F. Li, Improving the efficiency of solution processable organic photovoltaic devices by a star-shaped molecular geometry, J. Mater. Chem. 18 (2008) 4085–4090.

[41] M. Xu, R. Li, N. Pootrakulchote, D. Shi, J. Guo, Z. Yi, S.M. Zakeeruddin, M. Grätzel, P. Wang, Energy level and molecular engineering of organic D-p-A sensitizers in dye sensitized solar cells, J. Phys. Chem. C 112 (2008) 19770–19776.

[42] Y.Y. Liang, D.Q. Feng, Y. Wu, S.T. Tsai, G. Li, C. Ray, L.P. Yu, Highly efficient solar cell polymers developed via fine tuning of structural and electronic properties, J. Am. Chem. Soc. 131 (2009) 7792–7799.

[43] Y.J. Kim, K.H. Park, J.J. Ha, D.S. Chung, Y.H. Kim, C.E. Park, The effect of branched versus linear alkyl side chains on the bulk heterojunction photovoltaic performance of small molecules containing both benzodithiophene and thienopyrroledione, Phys. Chem. Chem. Phys. 16 (2014) 19874–19883.

[44] Y. Li, K. Yao, H.L. Yip, F.Z. Ding, Y.X. Xu, X. Li, Y. Chen, A.K.Y. Jen, Eleven membered fused ring low bandgap polymer with enhanced charge carrier mobility and photovoltaic performance, Adv. Funct. Mater. 24 (2014) 3631–3638.

[45] J.J.A. Chen, T.L. Chen, B.S. Kim, D.A. Poulsen, J.L. Mynar, J.M.J. Frechet, B. Ma, Quinacridone based molecular donors for solution processed bulk heterojunction organic solar cells, ACS Appl. Mater. Interfaces 2 (2010) 2679–2686.

[46] L. Biniek, C.L. Chochos, N. Leclerc, G. Hadziioannou, J.K. Kalitsis, R. Bechara, P. Leveque, T.A. Heiser, A [3,2-b]thienothiophene-alt-benzothiadiazole copolymer for photovoltaic applications: design, synthesis, material characterization and device performances, J. Mater. Chem. 19 (2009) 4946–4951.

[47] Y. Liang, D. Feng, Y. Wu, S.T. Tsai, G. Li, C. Ray, L. Yu, Highly efficient solar cell polymers developed via fine tuning of structural and electronic properties, J. Am. Chem. Soc. 131 (2009) 7792–7799.

[48] T. Aernouts, W. Geens, J. Poortmans, P. Heremans, S. Borghs, R. Mertens, Extraction of bulk and contact components of the series resistances in organic bulk donor acceptor heterojunctions, Thin Solid Films 403 (404) (2002) 297–301.

[49] P. Dutta, W. Yang, S.M. Eom, S.H. Lee, Synthesis and characterization of triphenylamine flanked thiazole based small molecules for high performance solution processed solar cells, Org. Elect. 13 (2012) 273–282.

[50] T. Ameri, P. Khoram, J. Min, C.J. Brabec, Organic ternary solar cells: a review, Adv. Mater. 25 (2013) 4245–4266.

[51] R. Shivanno, S. Shoaee, S. Dimitrov, S.K. Kanadappa, S. Rajaram, J.R. Durrant, K.S. Narayan, Charge generation and transport in efficient organic bulk heterojunction solar cells with a perylene acceptor, Energy Environ. Sci. 7 (2014) 435–441.

[52] S.D. Dimitrov, J.R. Durrant, Material design consideration for charge generation in organic solar cells, Chem. Mater. 26 (2014) 616–639.

[53] C.M. Proctor, C. Kim, D. Neher, T.Q. Nguyen, Nongerminate recombination and charge transport limitations in diketopyrrolopyrrole based solution processed small molecule solar cells, Adv. Funct. Mater. 23 (2013) 3584–3594.

[54] A.C. Stuart, J.R. Tumbleston, H. Zhou, W. Li, S. Liu, H. Ade, W. You, Fluorine substituent reduce charge recombination and drive structure and morphology development in polymer solar cells, J. Am. Chem. Soc. 135 (2013) 1806–1815.

[55] J.R. Tumbleston, A.C. Stuart, E. Gann, W. You, H. Ade, Fluorinated polymer yield high organic solar cell performance for a wide range of morphologies, Adv. Funct. Mater. 23 (2013) 3463–3470.

[56] D. Deng, Y. Zhang, L. Yuan, C. He, K. Lu, Z. Wei, Effects of shorted alkyl chains on solution processable small molecules with oxo-alkylated nitrile end capped acceptors for high performance organic solar cells, Adv. Energy Mater. (2014) 1400538, http://dx.doi.org/10.1002/aenm.201400538.

[57] C. Ji, L. Yin, L. Wang, T. Jia, S. Meng, Y. Sun, Y. Li, Linkage effects of linear D-p-A-p-D type diketopyrrolopyrrole triphenylamine based solution processable organic small molecule photovoltaic material, J. Mater. Chem. C 2 (2014) 4019–4026.

[58] H. Gao, Y. Li, L. Wang, C. Ji, Y. Wang, W. Tian, X. Yang, L. Yin, High performance asymmetrical push–pull small molecules end-capped with cyanophenyl for solution processed solar cells, Chem. Commun. 50 (2014) 10251–102554.

[59] L. Ye, S.Q. Zhang, L.J. Huo, M.J. Zhang, J.H. Hou, Molecular design toward highly efficient photovoltaic polymers based on two-dimensional conjugated benzodithiophene, Acc. Chem. Res. 47 (2014) 1595–1603.

[60] D.A. Vithanage, A. Devizis, V. Abramavicius, Y. Infahsaeng, D. Abramavicius, R.C.I. MacKenzie, P.E. Keivanidis, A. Yartsev, D. Hertel, J. Nelson, V. Sundstrom, J.V. Gulbinas, Visualizing charge separation in bulk heterojunction organic solar cells, Nat. Commun. (2013), http://dx.doi.org/10.1038/ncomms3334.

[61] H. Hoppe, N.S. Sariciftci, Morphology of polymer/fullerene bulk heterojunction solar cells, J. Mater. Chem. 16 (2006) 45–61.

[62] X.N. Yang, J. Loos, S.C. Veenstra, W.J.H. Verhees, M.M. Wienk, J.M. Kroon, M.A. Michels, R.A.J. Janssen, Nanoscale morphology of high performance polymer solar cells, Nano Lett. 5 (2005) 579–583.

[63] J.E. Slota, X. He, W.T.S. Huck, Controlling nanoscale morphology in polymer photovoltaic devices, Nano Today 5 (2010) 231–242.

[64] J. Peet, M.L. Senatore, A.J. Heeger, G.C. Bazan, The role of processing in the fabrication and optimization of plastic solar cells, Adv. Mater. 21 (2009) 1521–1527.

[65] H.Y. Chen, J.H. Hou, S.Q. Zhang, Y.Y. Liang, G.W. Yang, Y. Yang, L.P. Yu, Y. Wu, G. Li, Polymer solar cells with enhanced open circuit voltage and efficiency, Nat. Photon. 3 (2009) 649–653.

[66] T.Y. Chu, J. Lu, S. Beaupre, Y. Zhang, J.R. Pouliot, S. Wakim, J. Zhou, M. Leclerc, Z. Li, J. Ding, Y. Tao, Bulk heterojunction solar cells using thieno[3,4-c]pyrrole-4,6-dione and dithieno[3,2-b:2$^{\prime}$,3$^{\prime}$-d]silole copolymer with a power conversion efficiency of 7.3%, J. Am. Chem. Soc. 133 (2011) 4250–4253.

[67] Y. Liang, Z. Xu, J. Xia, S.T. Tsai, Y. Wu, G. Li, C. Ray, L. Yu, For the bright future – bulk heterojunction polymer solar cells with power conversion efficiency of 7.4%, Adv. Mater. 22 (2010) E135–E138.

[68] J.M. Szarko, J.C. Guo, Y.Y. Liang, B. Lee, B.S. Rolczynski, J. Strzalka, T. Xu, S. Loser, T.J. Marks, L.P. Yu, L.X. Chen, When function follows form: effects of donor copolymer side chains on film morphology and BHJ solar cell performance, Adv. Mater. 22 (2010) 5468–5472.

[69] L.A. Perez, J.T. Rogers, M.A. Brady, Y. Sun, G.C. Welch, K. Schmidt, M.F. Toney, H. Jinnai, A.J. Heeger, M.L. Chabinyc, G.C. Bazan, E.J. Kramer, The role of solvent additive processing in high performance in high performance small molecule solar cells, Chem. Mater. 26 (2014) 6531–6541.

[70] J.A. Love, S.D. Collins, I. Nagao, S. Mukherjee, H. Ade, G.C. Bazan, T.Q. Nguyen, Interplay of solvent additive concentration and active layer thickness on the performance of small molecule solar cells, Adv. Mater. 26 (2014) 7308–7316.

[71] A. Sharenko, N.D. Treat, J.A. Love, M.F. Toney, N. Stingelin, T.Q. Nquyen, Use of a commercially available nucleating agent to control the morphology development of solution processed small molecule bulk heterojunction organic solar cells, J. Mater. Chem. A 2 (2014) 15717–15721.

[72] M.S. Su, C.Y. Kuo, M.C. Yuan, U.S. Jeng, C.J. Su, K.H. Wei, Improving device efficiency of polymer/fullerene bulk heterojunction solar cells through enhanced crystallinity and reduced grain boundaries induced by solvent additives, Adv. Mater. 23 (2011) 3315–3319.

[73] J.T. Rogers, K. Schmidt, M.F. Toney, E.J. Kramer, G.C. Bazan, Structural order in bulk heterojunction films prepared with solvent additives, Adv. Mater. 23 (2011) 2284–2288.

[74] C.M. Proctor, M. Kuik, T.Q. Nguyen, Charge carrier recombination in organic solar cells, Prog. Polym. Sci. 38 (2013) 1941–1960.

[75] P.W.M. Blom, V.D. Mihailetchi, L.J.A. Koster, D.E. Markov, Device physics of polymer: fullerene heterojunction solar cells, Adv. Mater. 19 (2007) 1551–1566.

[76] A. Guerrero, S. Loser, G. Garcia-Belmonte, C.J. Bruns, J. Smith, H. Miyauchi, S.I. Stupp, J. Bisquert, T.J. Marks, Solution processed small molecule: fullerene bulk heterojunction solar cells: impedance spectroscopy deduced bulk and interfacial limits to fill factors, Phys. Chem. Chem. Phys. 15 (2013) 16456–16462.

[77] Z. He, C. Zhong, X. Huang, W.Y. Wong, H. Wu, L. Chen, S. Su, Y. Cao, Simultaneous enhancement of open circuit voltage, short circuit current density, and fill factor in polymer solar cells, Adv. Mater. 23 (2011) 4636–4643.